Theoretical Analysis of Seepage Field Distribution Induced by Pre-Excavation Dewatering Considering the Thickness of Waterproof Curtain and Delayed Responses of Water Table

Donglin Meng[1,2], Jingjing Han[1,*], Wenkai Lei[1,*], Haifeng Zhang[3] and Changzan Guan[1]

[1] School of Architecture and Electrical Engineering, Hezhou University, Hezhou, 542899, China

[2] Guangxi University Engineering Research Center for Green and Low-Carbon Urban Regeneration Construction, Hezhou, 542899, China

[3] Guangxi Construction Engineering Group No. 3 Construction Engineering Co., Ltd., Liuzhou, 545001, China

INFORMATION

Keywords:
Semi-analytical solution
pre-excavation dewatering
phreatic surface
unsteady-state seepage

DOI: 10.23967/j.rimni.2025.10.71762

SCIPEDIA Revista Internacional de Métodos Numéricos para Cálculo y Diseño en Ingeniería

Revista Internacional Métodos numéricos para cálculo y diseño en ingeniería RIMNI

In cooperation with CIMNE

Theoretical Analysis of Seepage Field Distribution Induced by Pre-Excavation Dewatering Considering the Thickness of Waterproof Curtain and Delayed Responses of Water Table

Donglin Meng[1,2], **Jingjing Han**[1,*], **Wenkai Lei**[1,*], **Haifeng Zhang**[3] **and Changzan Guan**[1]

[1]School of Architecture and Electrical Engineering, Hezhou University, Hezhou, 542899, China

[2]Guangxi University Engineering Research Center for Green and Low-Carbon Urban Regeneration Construction, Hezhou, 542899, China

[3]Guangxi Construction Engineering Group No. 3 Construction Engineering Co., Ltd., Liuzhou, 545001, China

ABSTRACT

Dewatering during foundation pit excavation generates substantial hydraulic gradients, potentially causing significant seepage forces at the excavation bottom, which threaten structural stability. To mitigate such risks, suspended waterproof curtains have been widely employed to elongate seepage paths and reduce groundwater flow velocities. However, accurately predicting seepage field, especially under transient groundwater conditions with phreatic surfaces and varying curtain geometries, remains challenging. This study develops a theoretical model addressing transient groundwater seepage in foundation pits, explicitly considering a moving phreatic surface, curtain penetration depth and thickness. The proposed analytical solution is validated against experimental results and numerical simulations performed using COMSOL Multiphysics. Parametric analyses reveal that decreasing the vertical distance between the retaining wall base and the impermeable layer from 30 to 10 m reduces external groundwater drawdown by approximately 52%. Additionally, thicker waterproof curtains markedly decrease internal drawdown magnitudes, redirect seepage pathways, and effectively lower external groundwater depletion. Analyses on specific yield reveal delayed water release significantly moderates drawdown rates, reducing ultimate drawdown magnitudes. Furthermore, elevated internal excavation water levels intensify hydraulic head differences, substantially extending seepage-affected zones and amplifying drawdown responses both inside and outside the foundation pit. Overall, these findings provide critical theoretical insights for optimizing foundation pit design and improving dewatering practices, ensuring excavation safety and mitigating environmental impacts.

OPEN ACCESS

Received: 11/08/2025

Accepted: 05/11/2025

Accepted: 03/02/2026

DOI
10.23967/j.rimni.2025.10.71762

Keywords:
Semi-analytical solution
pre-excavation dewatering
phreatic surface
unsteady-state seepage

1 Introduction

During foundation pit excavation, dewatering induces a significant hydraulic head difference between the inside and outside of the pit, resulting in a strong upward seepage force at the pit bottom.

*Correspondence: Jingjing Han, Wenkai Lei (201600006@hzxy.edu.cn, 1710402003@st.gxu.edu.cn).

Such a hydraulic condition can readily trigger piping and soil boiling, thereby undermining the stability and safety of the foundation pit [1,2]. In addition, dewatering inside foundation pit inevitably causes a drawdown of the surrounding groundwater level, which may induce regional ground settlement and consequently affect the serviceability of adjacent buildings [3,4]. The suspended waterproof curtain has been widely adopted in foundation pit engineering. It can ensure construction safety by extending the groundwater seepage path and reducing the seepage velocity, thereby mitigating the adverse effects of dewatering on existing infrastructure [5]. Therefore, accurately determining the distribution of the seepage field inside and outside the foundation pit under the protection of a suspended waterproof curtain is of great importance for ensuring construction safety.

Given the advantages of theoretical modeling in computational efficiency and general applicability, numerous studies have focused on developing analytical frameworks to address a wide range of problems in geotechnical engineering [6,7]. Previous seepage analyses typically employed simplified boundary conditions, in which the hydraulic head along the external boundary was assumed to remain constant due to sufficient and continuous groundwater recharge. Early studies mainly focused on steady-state seepage fields and solved two-dimensional problems using classical analytical techniques such as conformal mapping and Fourier transform methods [8]. Subsequent studies have introduced more practical complexities into the analytical models, including variations in curtain thickness [9] and the presence of stratified aquifers [10]. Nevertheless, transient seepage conditions are commonly encountered in practice, particularly in fine-grained soils with low permeability, where hydraulic equilibrium requires a prolonged period to be achieved. To address such scenarios, Li et al. [11] developed consolidation-based analytical solutions for evaluating excess pore-water pressure dissipation.

In excavation projects near the ocean or rivers, the shallow aquifer is affected by water-level fluctuations caused by waves, tides, etc. Consequently, the hydraulic head for the outside of the foundation pit should not be regarded as a constant, and the corresponding seepage problems have been investigated extensively. Many researchers deem such boundary can be treated as a varying hydraulic head boundary following harmonic oscillations, and have provided theoretical solutions under corresponding conditions by taking into account factors like soil anisotropy [12], the thickness of waterproof curtain [13], and excavation bottom sealing [14].

Conversely, foundation pits in inland regions often encounter conditions with limited groundwater recharge, making the phreatic surface (the unconfined aquifer boundary) a key factor controlling the seepage behavior. Accurately identifying and modeling the location and evolution of this free surface are therefore essential for reliable seepage analysis. Early studies based on the Boussinesq equation laid the theoretical foundation for understanding the evolution of the phreatic surface under fluctuating water levels [15,16]. Yu et al. [17] proposed analytical solutions to approximate steady-state seepage fields considering phreatic boundaries, although simplifying assumptions such as treating these boundaries as impermeable and neglecting curtain thickness limited their applicability. More advanced approaches, exemplified by Neuman's theory, introduced a linearized conceptualization of the phreatic aquifer as a moving interface, incorporating vertical flow components, elastic aquifer storage, and gravity-driven yield processes [18,19]. Neuman's model accurately captures the transient water-table response and has been successfully applied to interpret aquifer-system responses to groundwater extraction [20]. Despite these advancements, a systematic analytical approach simultaneously accounting for transient phreatic surface dynamics and retaining-wall geometry (particularly wall thickness) has not yet been comprehensively addressed.

Although numerical methods such as the finite element method (FEM) are widely applied to analyze transient seepage, they often rely heavily on mesh discretization and case-specific boundary

settings, which may obscure the underlying mechanisms and reduce computational efficiency in long-term simulations. Semi-analytical approaches, by contrast, retain an explicit analytical structure in the transform domain, which provides clearer physical insight into parameter influences and mitigates artificial boundary effects induced by meshing. These features make semi-analytical solutions particularly suitable for systematic parametric analyses and preliminary design evaluations.

In this paper, a semi-analytical solution is developed for the unsteady seepage field of a foundation pit considering the presence of a phreatic surface. The effects of key parameters, including the penetration depth and thickness of the suspended waterproof curtain, are incorporated into the formulation. The accuracy of the proposed solution is validated through comparisons with both laboratory experiments and numerical simulations conducted using COMSOL Multiphysics. Furthermore, the influences of the curtain thickness, specific yield, and other governing factors on groundwater drawdown are systematically investigated through parametric analyses.

2 Mathematical Model

2.1 Model Description

In excavation projects where the foundation pit exhibits a pronounced longitudinal shape—namely, its length far exceeds its width—the groundwater flow within cross-sectional planes perpendicular to the long axis can be idealized as a two-dimensional problem [4,10]. For simplicity, a symmetric half-domain is typically adopted for modeling purposes, as illustrated in Fig. 1a. The total hydraulic heads on the exterior and interior sides of the pit are denoted by h_o and h_i, respectively. The parameters b and d correspond to the foundation pit width and the thickness of the waterproof curtain. The effective lateral extent of seepage influence is defined as $l - (b + d)$, and the vertical separation between the bottom of the curtain and the top of the underlying impermeable stratum is represented by h_c. The coordinate system is defined with x and z as the horizontal and vertical directions, where x is positive to the right and z is positive upward. Assuming Darcy flow conditions prevail both inside and outside the excavation, the domain is divided into three distinct seepage zones (Zone I, Zone II, and Zone III) based on the flow boundaries adjacent to the curtain interface. In addition, a systematic flowchart (see Fig. 1b) has been incorporated to provide a clearer and more intuitive representation of the overall research methodology.

2.2 Governing Equations and Solving Conditions

Based on the above physical descriptions and modeling assumptions, the transient seepage process in Zones I, II, and III is governed by the following equations:

$$k_h \frac{\partial^2 s_i}{\partial x^2} + k_v \frac{\partial^2 s_i}{\partial z^2} = S_s \frac{\partial s_i}{\partial t}, \quad (i = 1, 2, 3) \tag{1}$$

where s_i is drawdown and $i = 1$, 2, and 3 denote the zones I, II and III in unconfined aquifer, respectively; k_h and k_v are horizontal and vertical hydraulic conductivities, respectively; S_s is specific storage; parameter t is time coordinate.

In Zone I, considering the model symmetry and the assumption that the waterproof curtain acts as a perfect barrier to flow, the horizontal boundary conditions are defined as follows:

$$\left.\frac{\partial s_1}{\partial x}\right|_{x=0} = 0 \tag{2a}$$

and

$$\left.\frac{\partial s_1}{\partial x}\right|_{x=b} = 0, \quad (h_c < z \leq h_i) \tag{2b}$$

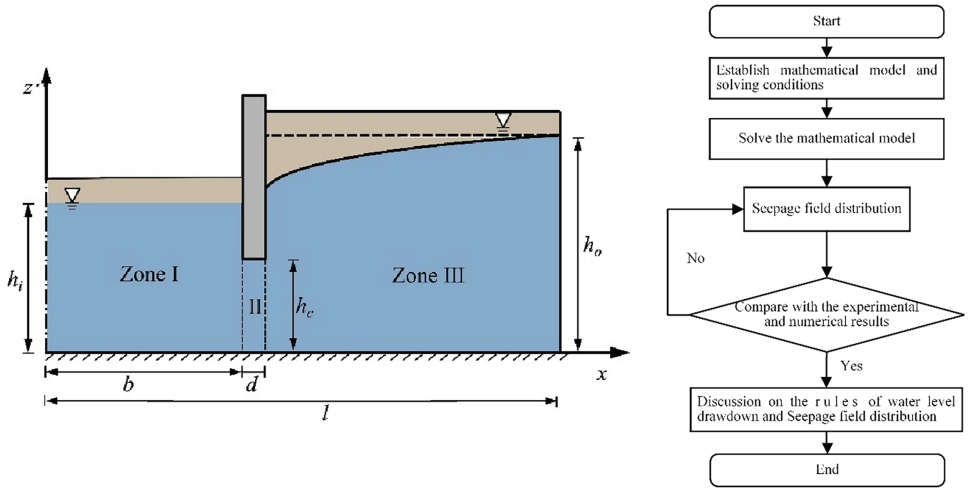

(**a**) (**b**)

Figure 1: (**a**) Two-dimensional analysis model for a long-narrow foundation pit system. (**b**) Flowchart for water level drawdown and seepage field distribution induced by pre-excavation dewatering

In real engineering applications, defects or heterogeneities in the curtain may permit a certain degree of seepage, which can cause actual drawdown to exceed the values predicted by the ideal impermeable assumption. Future extensions of the present framework could relax this assumption by introducing partially permeable boundary conditions to better represent practical situations.

At the interface between Zones I and II, a Cauchy-type boundary condition is imposed to ensure continuity, that is:

$$s_1|_{x=b} = s_2|_{x=b}, \quad (0 < z \leq h_c) \tag{3a}$$

and

$$\left.\frac{\partial s_1}{\partial x}\right|_{x=b} = \left.\frac{\partial s_2}{\partial x}\right|_{x=b}, \quad (0 \leq z \leq h_c) \tag{3b}$$

Within the foundation pit, the upper boundary is maintained at a fixed hydraulic head, while the lower boundary is assumed to be impermeable. Accordingly, the vertical boundary conditions are specified as follows:

$$\left.\frac{\partial s_1}{\partial z}\right|_{z=0} = 0 \tag{4a}$$

and

$$s_1|_{z=h_i} = \Delta h \tag{4b}$$

where $\Delta h = h_o - h_i$.

For Zone II, continuity across the interface with Zone I is governed by Eqs. (3a) and (3b), while the condition ensuring continuity at the boundary between Zones II and III can be expressed as:

$$s_2|_{x=(b+d)} = s_3|_{x=(b+d)}, \quad (0 < z \le h_c) \tag{5a}$$

and

$$\left.\frac{\partial s_2}{\partial x}\right|_{x=(b+d)} = \left.\frac{\partial s_3}{\partial x}\right|_{x=(b+d)}, \quad (0 \le z \le h_c) \tag{5b}$$

Both the top and bottom boundaries of zone II are considered impervious, ones can get

$$\left.\frac{\partial s_2}{\partial z}\right|_{z=0} = 0 \tag{6a}$$

and

$$\left.\frac{\partial s_2}{\partial z}\right|_{z=h_c} = 0 \tag{6b}$$

For zone III, the horizontal boundary condition can be described as

$$\left.\frac{\partial s_3}{\partial x}\right|_{x=(b+d)} = 0, \quad (h_c < z \le h_0) \tag{7a}$$

And the continuity condition at the interface of zones II and III satisfies Eqs. (5a) and (5b).

$$s_3|_{x=l} = 0 \tag{7b}$$

The impervious boundary at the bottom of zone III can be expressed as

$$\left.\frac{\partial s_3}{\partial z}\right|_{z=0} = 0 \tag{8a}$$

A phreatic surface is employed to simulate the top boundary outside foundation pit, Neuman [18,19] treated the water table as a movable material interface and presented a linearized model for the unconfined aquifers, under the assumption that the water table decline is significantly smaller than the original aquifer thickness. That is

$$\left.\left(S_Y\frac{\partial s_3}{\partial t} + k_v\frac{\partial s_3}{\partial z}\right)\right|_{z=h_o} = 0 \tag{8b}$$

where S_Y is the specific yield of the unconfined aquifer describing the recharge rate to the saturated aquifer per unit length of water table decline.

It should be noted that the feasibility of Neuman boundary has been confirmed by several recent studies on dewatering [5,20,21].

Prior to the commencement of dewatering, the aquifer is assumed to be at its initial equilibrium, with zero drawdown throughout. The initial conditions for all three zones are thus defined as follows:

$$s_1|_{t=0} = s_2|_{t=0} = s_3|_{t=0} = 0 \tag{9}$$

3 Solving Procedures

3.1 Boundary Transform

The presence of Cauchy-type boundaries at $x = b$ and $x = (b + d)$ introduces mixed boundary conditions for the variables s_i, which renders the direct application of the integral transform method infeasible. To overcome this challenge, the present study adopts the boundary transformation technique introduced by Chen et al. [22,23], which converts these mixed boundaries into a standardized form amenable to analytical treatment. The effectiveness of this approach has been demonstrated in several recent studies [7,24,25].

Accordingly, the horizontal boundary conditions for s_i at $x = b$ and $x = (b + d)$ after transformation can be expressed as follows:

$$\left.\frac{\partial s_1}{\partial x}\right|_{x=b} = \begin{cases} -q_1(z,t), & (0 \le z \le h_c) \\ 0, & (h_c < z \le h_i) \end{cases} \tag{10a}$$

$$\left.\frac{\partial s_2}{\partial x}\right|_{x=b} = -q_1(z,t) \tag{10b}$$

$$\left.\frac{\partial s_2}{\partial x}\right|_{x=(b+d)} = -q_2(z,t) \tag{10c}$$

and

$$\left.\frac{\partial s_3}{\partial x}\right|_{x=(b+d)} = \begin{cases} -q_2(z,t), & (0 \le z \le h_c) \\ 0, & (h_c < z \le h_o) \end{cases} \tag{10d}$$

where the transformed variables $q_1(z,t)$ and $q_2(z,t)$ can be determined using Eqs. (3a) and (5a).

3.2 Solution of Drawdown for Different Zones

Upon performing a Laplace transform with respect to time and incorporating the initial condition given in Eq. (9), the governing equations and associated conditions can be reformulated in the frequency domain. The solution process for each zone is then outlined as follows:

For Zone I, the transformed governing equation and corresponding boundary conditions in the Laplace domain are given by

$$k_h \frac{\partial^2 \bar{s}_1}{\partial x^2} + k_v \frac{\partial^2 \bar{s}_1}{\partial z^2} = S_s p \bar{s}_1 \tag{11}$$

$$\left.\frac{\partial \bar{s}_1}{\partial x}\right|_{x=0} = 0 \tag{12a}$$

and

$$\left.\frac{\partial \bar{s}_1}{\partial x}\right|_{x=b} = \begin{cases} -\bar{q}_1(z,p), & (0 \le z \le h_c) \\ 0, & (h_c < z \le h_i) \end{cases} \tag{12b}$$

$$\left.\frac{\partial \bar{s}_1}{\partial z}\right|_{z=0} = 0 \tag{13a}$$

and

$$\bar{s}_1|_{z=h_i} = \frac{\Delta h}{p} \tag{13b}$$

where p is the Laplace transform parameter; $\bar{s}_1 = \int_0^\infty s_1 e^{-pt} dt$; $\bar{q}_1 = \int_0^\infty q_1 e^{-pt} dt$.

It is apparent that the vertical boundary specified in Eq. (13b) is inhomogeneous. To facilitate the application of integral transforms, the substitution $\bar{s}_1 = w + \Delta h/p$ is introduced, thereby converting the boundary condition into a homogeneous form. Subsequently, the finite Fourier cosine transform is employed on the modified governing equation and the associated horizontal boundary conditions, resulting in:

$$\frac{\partial^2 \tilde{w}}{\partial x^2} - \beta_m^2(p)\frac{\tilde{w}}{b^2} = -\frac{\beta_m^2(p)}{b^2}\varphi_m(p) \tag{14}$$

$$\left.\frac{\partial \tilde{w}}{\partial x}\right|_{x=0} = 0 \tag{15a}$$

and

$$\left.\frac{\partial \tilde{w}}{\partial x}\right|_{x=b} = -\int_0^{h_c} \bar{q}_1(z,p)\cos\left(\frac{M_m z}{h_i}\right) dz \tag{15b}$$

where $\beta_m^2(p) = k_v b^2 M_m^2/\left(k_h h_i^2\right) + b^2 S_s p/k_h$; $\varphi_m(p) = (-1)^m h_i^3 \Delta h S_s/(k_v M_m^3 + M_m S_s p h_i^2)$; $\tilde{w}(x,m,p) = \int_0^{h_c} w(x,z,p)\cos(M_m z/h_i)\,dz$, $M_m = (2m-1)\pi/2, m = 1,2,3\ldots$

It is evident that Eq. (14) constitutes a second-order ordinary differential equation with constant coefficients. By applying the horizontal boundary conditions specified in Eqs. (15a) and (15b), an explicit solution can be obtained as follows:

$$\tilde{w} = \varphi_m(p) - \frac{b\cosh\left(\beta_m(p)\frac{x}{b}\right)}{\beta_m(p)\sinh(\beta_m(p))}\int_0^{h_c} \bar{q}_1(z,p)\cos\left(\frac{M_m z}{h_c}\right) dz \tag{16}$$

The drawdown solution in Zone I within the Laplace domain is recovered by first performing the inverse finite Fourier cosine transform on the result of Eq. (16), followed by the necessary variable substitution. This procedure yields the following expression:

$$\bar{s}_1 = \frac{\Delta h}{p} + \frac{2}{h_i}\sum_{m=1}^{\infty}\varphi_m(p)\cos\left(M_m\frac{z}{h_i}\right) \tag{17}$$

$$-\frac{2}{h_i}\sum_{m=1}^{\infty}\frac{b\cosh\left(\beta_m(p)\frac{x}{b}\right)}{\beta_m(p)\sinh(\beta_m(p))}\cos\left(M_m\frac{z}{h_i}\right)\int_0^{h_c}\bar{q}_1(z,p)\cos\left(\frac{M_m z}{h_i}\right) dz$$

For zones II, the governing equation and the boundary conditions in frequency domain can be expressed as follows:

$$k_h\frac{\partial^2 \bar{s}_2}{\partial x^2} + k_v\frac{\partial^2 \bar{s}_2}{\partial z^2} = S_s p \bar{s}_2 \tag{18}$$

$$\left.\frac{\partial \bar{s}_2}{\partial x}\right|_{x=b} = -\bar{q}_1(z,t) \tag{19a}$$

and

$$\left.\frac{\partial \bar{s}_2}{\partial x}\right|_{x=(b+d)} = -\bar{q}_2(z,t) \tag{19b}$$

$$\left.\frac{\partial \bar{s}_2}{\partial z}\right|_{z=0} = 0 \tag{20a}$$

and

$$\left.\frac{\partial \bar{s}_2}{\partial z}\right|_{z=h_c} = 0 \tag{20b}$$

where $\bar{s}_2 = \int_0^\infty s_2 \mathrm{e}^{-pt}\mathrm{d}t$; $\bar{q}_2 = \int_0^\infty q_2 \mathrm{e}^{-pt}\mathrm{d}t$.

According to the form of vertical boundary conditions of Eqs. (20a) and (20b), the governing equation of Eq. (18) and horizontal boundary conditions of Eqs. (19a) and (19b) are transformed using the finite cosine transform as follows:

$$\frac{\partial^2 \widetilde{\bar{s}}_2}{\partial x^2} - \frac{\zeta_m^2(p)}{d^2}\widetilde{\bar{s}}_2 = 0 \tag{21}$$

$$\left.\frac{\partial \widetilde{\bar{s}}_2}{\partial x}\right|_{x=b} = -\int_0^{h_c} \bar{q}_1(z,p)\cos\left(\frac{\mu_m z}{h_c}\right)dz \tag{22a}$$

and

$$\left.\frac{\partial \widetilde{\bar{s}}_2}{\partial x}\right|_{x=(b+d)} = -\int_0^{h_c} \bar{q}_2(z,p)\cos\left(\frac{\mu_m z}{h_c}\right)dz \tag{22b}$$

where $\zeta_m^2(p) = k_\mathrm{v} d^2 \mu_m^2 / \left(k_\mathrm{h} h_\mathrm{c}^2\right) + S_\mathrm{s} p d^2 / k_\mathrm{h}$; $\widetilde{\bar{s}}_2(x,m,p) = \int_0^{h_c} \bar{s}_2(x,z,p)\cos\left(\mu_m z/h_\mathrm{c}\right)\mathrm{d}z$; $\mu_m = m\pi$, $m = 0,1,2,3\ldots$

Eq. (21) represents a second-order homogeneous differential equation with constant coefficients. By incorporating the horizontal boundary conditions outlined in Eqs. (22a) and (22b), its solution can be derived as follows:

$$\widetilde{\bar{s}}_2 = \frac{d}{\zeta_m(p)\sinh(\zeta_m)}\left[A_m \cosh\left(\zeta_m \frac{(b+d)-x}{d}\right) - B_m \cosh\left(\zeta_m \frac{b-x}{d}\right)\right] \tag{23}$$

where $A_m(p) = \int_0^{h_c} \bar{q}_1(z,p)\cos\left(\mu_m z/h_\mathrm{c}\right)\mathrm{d}z$; $B_m = \int_0^{h_c} \bar{q}_2(z,p)\cos\left(\mu_m z/h_\mathrm{c}\right)\mathrm{d}z$.

Taking the inverse finite cosine transform to Eq. (23), the Laplace-domain solution of drawdown in zone II can be obtained, i.e.,

$$\bar{s}_2 = \frac{2}{\delta_m h_c}\sum_{m=0}^{\infty} \frac{d\cos\left(\mu_m \frac{z}{h_c}\right)}{\zeta_m(p)\sinh(\zeta_m(p))}\left[A_m \cosh\left(\zeta_m \frac{(b+d)-x}{d}\right) - B_m \cosh\left(\zeta_m \frac{b-x}{d}\right)\right] \tag{24}$$

where $\delta_m = \begin{cases} 2, & m = 0 \\ 1, & m \neq 0 \end{cases}$.

For zones III, the governing equation and the boundary conditions in frequency domain can be expressed as follows:

$$k_h \frac{\partial^2 \bar{s}_3}{\partial x^2} + k_v \frac{\partial^2 \bar{s}_3}{\partial z^2} = S_s p \bar{s}_3 \tag{25}$$

$$\left.\frac{\partial \bar{s}_3}{\partial x}\right|_{x=(b+d)} = \begin{cases} -\bar{q}_2(z,p), & (0 \le z \le h_c) \\ 0, & (h_c < z \le h_o) \end{cases} \tag{26a}$$

and

$$\bar{s}_2|_{x=l} = 0 \tag{26b}$$

$$\left.\frac{\partial \bar{s}_3}{\partial z}\right|_{z=0} = 0 \tag{27a}$$

and

$$\left.\left(\frac{\partial \bar{s}_3}{\partial z} + \frac{S_Y p}{k_v}\bar{s}_3\right)\right|_{z=h_o} = 0 \tag{27b}$$

where $\bar{s}_3 = \int_0^\infty s_3 \mathrm{e}^{-pt} \mathrm{d}t$.

According to the form of vertical boundary conditions of Eqs. (27a) and (27b), the governing equation of Eq. (25) and horizontal boundary conditions of Eqs. (26a) and (26b) are transformed using the finite cosine transform as follows:

$$\frac{\partial^2 \widetilde{\bar{s}}_3}{\partial x^2} - \frac{\lambda_m^2(p)}{(l-b-d)^2}\widetilde{\bar{s}}_3 = 0 \tag{28}$$

$$\left.\frac{\partial \widetilde{\bar{s}}_3}{\partial x}\right|_{x=(b+d)} = -\int_0^{h_c} \bar{q}_2(z,p) \cos\left(\gamma_m \frac{z}{h_o}\right) dz \tag{29a}$$

and

$$\widetilde{\bar{s}}_3|_{x=l} = 0 \tag{29b}$$

where $\lambda_m^2(p) = \gamma_m^2 k_\mathrm{v} (l-b-d)^2 / \left(h_o^2 k_\mathrm{h}\right) + S_s p (l-b-d)^2 / k_\mathrm{h}$; $\widetilde{\bar{s}}_3(x,m,p) = \int_0^{h_o} \bar{s}_3(x,z,p) \cos(\gamma_m z/h_o)$ dz; parameter γ_m is the solution of the following equation, i.e.,

$$\frac{\gamma_m}{h_o}\tan(\gamma_m) - \frac{S_Y p}{k_v} = 0 \tag{30}$$

where $m = 1, 2, 3 \ldots$

The horizontal boundary conditions of Eqs. (29a) and (29b) can be used to solve the second-order homogeneous constant coefficient differential equation of Eq. (28). One can get

$$\widetilde{\bar{s}}_3 = C_m \left[\frac{1}{\cosh(\lambda_m(p))} \sinh\left(\frac{\lambda_m(p)(l-x)}{l-(b+d)}\right)\right] \frac{l-(b+d)}{\lambda_m(p)} \tag{31}$$

where $C_m = \int_0^{h_c} \bar{q}_2(z,p) \cos(\gamma_m z/h_\mathrm{o})\, \mathrm{d}z$.

Taking the inverse finite cosine transform to Eq. (31), the Laplace-domain solution of drawdown in zone III can be obtained, i.e.,

$$\bar{s}_3 = (l-b-d)\sum_{m=1}^{\infty}\frac{C_m\alpha_m(p)}{\lambda_m(p)}\frac{\sinh\left(\lambda_m(p)\dfrac{l-x}{l-(b+d)}\right)}{\cosh(\lambda_m(p))}\cos\left(\gamma_m\frac{z}{h_o}\right) \tag{32}$$

where $\alpha_m(p)$ can be expressed as follows:

$$\alpha_m(p) = \frac{2\left[(\gamma_m/h_o)^2 + (S_Y p/k_v)^2\right]}{h_o\left[(\gamma_m/h_o)^2 + (S_Y p/k_v)^2\right] + S_Y p/k_v}$$

It is apparent that the solutions provided in Eqs. (17), (24), and (32) still contain the unknown variables $\bar{q}_1(z,p)$ and $\bar{q}_2(z,p)$, preventing their direct application. Although the derivations employ the transformed boundary conditions from Eqs. (10a)–(10d), the original interface and boundary conditions (namely, Eqs. (3a) and (5a)) must also be fulfilled. Therefore, substituting the expressions from Eqs. (17), (24), and (32) into Eqs. (3a) and (5a) yields:

$$\begin{aligned}
&\frac{\Delta h}{p} + \frac{2}{h_i}\sum_{m=1}^{\infty}\varphi_m(p)\cos\left(M_m\frac{z}{h_i}\right)\\
&= \frac{2b}{h_i}\sum_{m=1}^{\infty}\frac{coth(\beta_m(p))}{\beta_m(p)}\cos\left(M_m\frac{z}{h_i}\right)\int_0^{h_c}\bar{q}_1(z,p)\cos\left(\frac{M_m z}{h_i}\right)dz\\
&+ \frac{2}{\delta_m h_c}\sum_{m=0}^{\infty}\frac{d\cos\left(\mu_m\dfrac{z}{h_c}\right)}{\zeta_m(p)\sinh(\zeta_m(p))}\left[\begin{array}{c}\cosh(\zeta_m(p))\int_0^{h_c}\bar{q}_1(z,p)\cos\left(\dfrac{\mu_m z}{h_c}\right)dz\\ -\int_0^{h_c}\bar{q}_2(z,p)\cos\left(\frac{\mu_m z}{h_c}\right)dz\end{array}\right]
\end{aligned} \tag{33a}$$

and

$$\begin{aligned}
&\frac{2}{\delta_m h_c}\sum_{m=0}^{\infty}\frac{d\cos\left(\mu_m\dfrac{z}{h_c}\right)}{\zeta_m(p)\sinh(\zeta_m(p))}\left[\int_0^{h_c}\bar{q}_1(z,p)\cos\left(\frac{\mu_m z}{h_c}\right)dz - \cosh(\zeta_m)\int_0^{h_c}\bar{q}_2(z,p)\cos\left(\frac{\mu_m z}{h_c}\right)dz\right]\\
&= (l-b-d)\sum_{m=1}^{\infty}\frac{\alpha_m(p)}{\lambda_m(p)}\tanh(\lambda_m(p))\cos\left(\gamma_m\frac{z}{h_o}\right)\int_0^{h_c}\bar{q}_2(z,p)\cos\left(\gamma_m\frac{z}{h_o}\right)dz
\end{aligned} \tag{33b}$$

It is important to emphasize that Eqs. (33a) and (33b) hold for any value of z within the interval $[0, h_c]$. However, owing to the transcendental form of these equations, explicit analytical solutions for $\bar{q}_1(z,p)$ and $\bar{q}_2(z,p)$ are generally unattainable. As shown in Fig. 2, to overcome this challenge, the local discretization method is used at the zone I-II interface boundary ($x = b$, $0 \le z \le h_c$) and the zones II–III interface boundary ($x = b + d$, $0 \le z \le h_c$), the validity of which has been confirmed by a number of recent investigations [26–28].

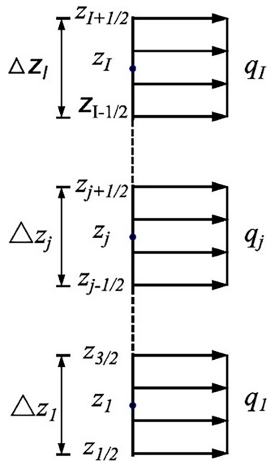

Figure 2: Local discretization for the boundary at $x = b$ and $x = b + d$.

The interval $[0, h_c]$ is divided into I segments, each with a length of Δz_j ($j \in [1, I]$). In each segment, the values of $\overline{q}_1(z,p)$ and $\overline{q}_2(z,p)$ are assumed to be constant, and the continuous variable $\overline{q}_1(z,p)$ and $\overline{q}_2(z,p)$ defined over the interval $[0, h_c]$, is replaced by discrete variables $\overline{q}_1^j(p)$ and $\overline{q}_2^j(p)$ at points $j \in [1, I]$. By doing so, the four integrals with unknown variable $\overline{q}_1(z,p)$ and $\overline{q}_2(z,p)$ can be rewritten in series form as follows:

$$\int_0^{h_c} \overline{q}_1(z,p) \cos\left(\frac{M_m z}{h_i}\right) dz = \frac{2h_i}{M_m} \sum_{j=1}^{I} \left[\sin\left(M_m \frac{\Delta z_j}{2h_i}\right) \cos\left(M_m \frac{z_j}{h_i}\right) \overline{q}_1^j(z_j,p)\right] \tag{34a}$$

$$\int_0^{h_c} \overline{q}_1(z,p) \cos\left(\frac{\mu_m z}{h_c}\right) dz = \begin{cases} \dfrac{2h_c}{\mu_m} \displaystyle\sum_{j=1}^{I} \left[\sin\left(\mu_m \frac{\Delta z_j}{2h_c}\right) \cos\left(\mu_m \frac{z_j}{h_c}\right) \overline{q}_1^j(z_j,p)\right], & (m \neq 0) \\ \displaystyle\sum_{j=1}^{I} \Delta z_j \overline{q}_1^j(z_j,p), & (m = 0) \end{cases} \tag{34b}$$

$$\int_0^{h_c} \overline{q}_2(z,p) \cos\left(\frac{\mu_m z}{h_c}\right) dz = \begin{cases} \dfrac{2h_c}{\mu_m} \displaystyle\sum_{j=1}^{I} \left[\sin\left(\mu_m \frac{\Delta z_j}{2h_c}\right) \cos\left(\mu_m \frac{z_j}{h_c}\right) \overline{q}_2^j(z_j,p)\right], & (m \neq 0) \\ \displaystyle\sum_{j=1}^{I} \Delta z_j \overline{q}_2^j(z_j,p), & (m = 0) \end{cases} \tag{34c}$$

$$\int_0^{h_c} \overline{q}_2(z,p) \cos\left(\gamma_m \frac{z}{h_o}\right) dz = \frac{2h_o}{\gamma_m} \sum_{j=1}^{I} \left[\sin\left(\gamma_m \frac{\Delta z_j}{2h_o}\right) \cos\left(\gamma_m \frac{z_j}{h_o}\right) \overline{q}_2^j(z_j,p)\right] \tag{34d}$$

where z_j = center coordinate of the jth segment.

By substituting Eqs. (34a)–(34d) into Eqs. (33a) and (33b), and evaluating Eq. (33) at $z = z_i$ ($i \in [1, I]$), the following relations are obtained:

$$\begin{bmatrix} a_1^{i,j} & a_2^{i,j} \\ a_3^{i,j} & a_4^{i,j} \end{bmatrix} \begin{bmatrix} \overline{q}_1^j(p) \\ \overline{q}_2^j(p) \end{bmatrix} = \begin{bmatrix} c_1^i \\ c_2^i \end{bmatrix} \tag{35}$$

where

$$a_1^{i,j} = \frac{d\coth\left(\zeta_0\left(p\right)\right)}{h_c\zeta_0\left(p\right)}\Delta z_j\overline{q}_1^j\left(z_j,p\right) + \sum_{m=1}^{\infty}\frac{4bcoth\left(\beta_m\left(p\right)\right)}{M_m\beta_m\left(p\right)}\sin\left(M_m\frac{\Delta z_j}{2h_i}\right)\cos\left(M_m\frac{z_j}{h_i}\right)\cos\left(M_m\frac{z_i}{h_i}\right)$$
$$+\sum_{m=1}^{\infty}\frac{4d\coth\left(\zeta_m\left(p\right)\right)}{\mu_m\zeta_m\left(p\right)}\sin\left(\mu_m\frac{\Delta z_j}{2h_c}\right)\cos\left(\mu_m\frac{z_j}{h_c}\right)\cos\left(\mu_m\frac{z_i}{h_c}\right)$$

$$a_2^{i,j} = \sum_{m=1}^{\infty}\frac{-4d}{\mu_m\zeta_m\left(p\right)\sinh\left(\zeta_m\left(p\right)\right)}\sin\left(\mu_m\frac{\Delta z_j}{2h_c}\right)\cos\left(\mu_m\frac{z_j}{h_c}\right)\cos\left(\mu_m\frac{z_i}{h_c}\right) - \frac{d}{h_c\zeta_0\left(p\right)\sinh\left(\zeta_0\left(p\right)\right)}\Delta z_j$$

$$a_3^{i,j} = \sum_{m=1}^{\infty}\frac{4d}{\mu_m\zeta_m\left(p\right)\sinh\left(\zeta_m\left(p\right)\right)}\sin\left(\mu_m\frac{\Delta z_j}{2h_c}\right)\cos\left(\mu_m\frac{z_j}{h_c}\right)\cos\left(\mu_m\frac{z_i}{h_c}\right) + \frac{d}{h_c\zeta_0\left(p\right)\sinh\left(\zeta_0\left(p\right)\right)}\Delta z_j$$

$$a_4^{i,j} = -\frac{dcoth\left(\zeta_0\right)}{h_c\zeta_0\left(p\right)}\Delta z_j + \sum_{m=1}^{\infty}\frac{-4dcoth\left(\zeta_m\left(p\right)\right)}{\mu_m\zeta_m\left(p\right)}\sin\left(\mu_m\frac{\Delta z_j}{2h_c}\right)\cos\left(\mu_m\frac{z_j}{h_c}\right)\cos\left(\mu_m\frac{z_i}{h_c}\right)$$
$$-\sum_{m=1}^{\infty}\frac{2h_o\left(l-b-d\right)\alpha_m\left(p\right)}{\lambda_m\left(p\right)\gamma_m coth\left(\lambda_m\left(p\right)\right)}\sin\left(\gamma_m\frac{\Delta z_j}{2h_o}\right)\cos\left(\gamma_m\frac{z_j}{h_o}\right)\cos\left(\gamma_m\frac{z_i}{h_o}\right)$$

$$c_1^i = \frac{\Delta h}{p} + \frac{2}{h_i}\sum_{m=1}^{\infty}\varphi_m\left(p\right)\cos\left(M_m\frac{z_i}{h_i}\right)$$

$$c_2^i = 0$$

After $\overline{q}_1^j\left(p\right)$ and $\overline{q}_2^j\left(p\right)$ is obtained through solving Eq. (35), the drawdown for zone I, zone II, and zone III in the Laplace domain is then obtained.

In most cases, Laplace transforms are applied to simplify the solution process for differential and integral equations; however, obtaining closed-form solutions in the time domain is often infeasible for complex engineering models. To address this limitation, various numerical inversion techniques for the Laplace transform have been developed. Among them, the Abate and Whitt algorithm [29] has proven to be a highly effective and efficient method for numerically retrieving time-domain solutions. Compared with classical schemes such as the Stehfest method [30], this algorithm provides more reliable accuracy for long-term responses and avoids the numerical oscillations often encountered in highly transient processes. Its error control is achieved through adaptive truncation of the Fourier expansion, which effectively balances computational cost and accuracy. Similar strategies have been successfully adopted in previous studies [31], and these works also provide detailed discussions on the stability and numerical performance of the algorithm, further confirming its suitability for the present analysis.

Overall, this study firstly develops a mathematical model to describe the seepage distribution caused by pre-excavation dewatering. To handle irregular boundaries, the computational domain was divided into regular three domains, and a boundary transformation technique was employed to convert mixed-type boundaries into a solvable form. Subsequently, Laplace and Fourier transforms were applied to reduce the governing equations, and numerical inverse Laplace transforms were used

to recover time-domain solutions. This systematic framework ensures a rigorous and effective semi-analytical solution, thereby improving the reliability and applicability of the proposed approach for dewatering system design in deep excavation projects.

4 Solution Evaluation

4.1 Experimental Data Validation

The present analytical solutions are validated by comparison with laboratory model experiment results, which provide a controlled environment for minimizing site-specific uncertainties such as sediment heterogeneity and variability in initial or boundary conditions [32,33]. This controlled setting makes model experiments particularly suitable for verification purposes. In this study, experimental data from Xue et al. [34] are adopted. According to their description, homogeneous sand was used to ensure repeatability and to represent the relatively high permeability of unconfined aquifers, with a coefficient of non-uniformity of 2.99 and approximately equal horizontal and vertical hydraulic conductivities. The relevant are summarized in Table 1, including specific storage $S_s = 1 \times 10^{-4}\,\mathrm{m}^{-1}$, specific yield $S_Y = 0.2$, and negligible curtain thickness ($d \to 0$). Fig. 3 presents a comparison of hydraulic head contour maps ($h = h_o - s$) derived from both the experimental measurements and theoretical predictions. The results show strong agreement between the theoretical equipotential lines and those observed experimentally, especially in regions near the pit base, thereby preliminarily demonstrating the correctness of the solution presented in this paper.

Table 1: Parameter values for experimental analysis

b/m	l/m	h_i/m	h_o/m	h_c/m	k_h/k_v
0.8	2.3	0.9	1.7	0.4	1

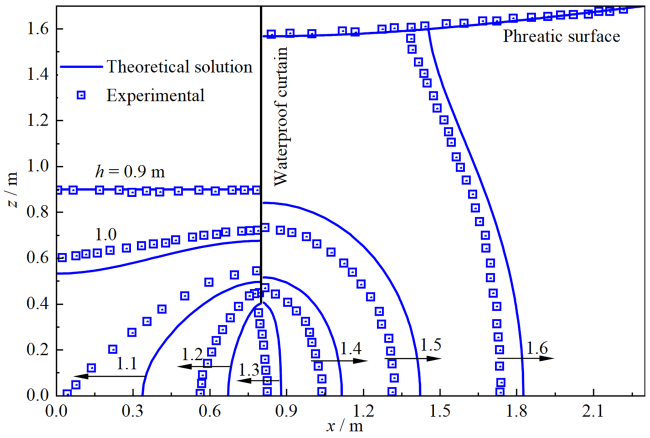

Figure 3: Comparison of the total hydraulic head in the unconfined aquifer obtained by the proposed method and experimental method

4.2 Comparison with Numerical Solution

COMSOL Multiphysics provides a robust and versatile platform for numerically approximating solutions to complex differential equations encountered in groundwater seepage analysis. In this

section, numerical simulations performed using COMSOL are employed to further evaluate the accuracy and validity of the proposed analytical model. The numerical model is built using a triangular mesh with a total of 6421 mesh elements. The minimum element size is 0.004 m and the maximum element size is 2 m. A transient solver is used, and the time step is manually entered by the user according to the requirements. All relevant computational parameters are specified in Table 2 to ensure comparability between the numerical and analytical results. Fig. 4 presents a direct comparison of the drawdown contour maps derived from the semi-analytical solution and those obtained from numerical simulations. The strong agreement observed between the two sets of contours across the computational domain serves to verify both the correctness and practical applicability of the developed solution for engineering analysis.

Table 2: Parameter values for numerical analysis

Parameter	Value	Parameter	Value
h_i	40 m	h_o	50 m
h_c	30 m	b	20 m
d	1 m	l	200 m
S_s	1×10^{-4} m^{-1}	S_Y	0.2
k_h	0.5 m/d	k_v	0.1 m/d

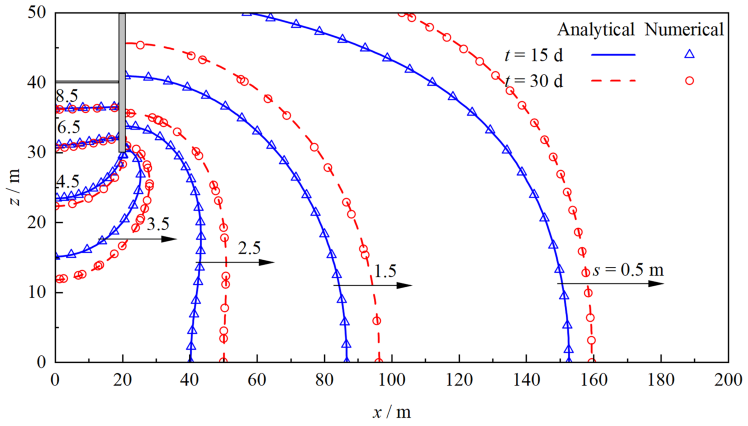

Figure 4: Comparison of the drawdown in the unconfined aquifer between analytical solution and numerical solution

Overall, the feasibility of the theoretical solution has been confirmed through comparison with experimental results (Fig. 3), while its correctness has been further verified by the strong agreement observed with numerical simulations (Fig. 4).

5 Parametric Study

In this section, a systematic evaluation is conducted to quantify the effects of key governing parameters on groundwater drawdown behavior. The analysis focuses on the penetration depth and thickness of the waterproof curtain, the specific yield (S_Y), and the internal water level parameter (h_i), which are known to significantly influence the seepage field within and around the foundation pit.

To ensure clarity and consistency in the comparative analysis, a baseline set of input parameters is provided in Table 2. For each individual parametric investigation, only the target parameter is varied while all other parameters are held constant at their reference values, thereby isolating the specific impact of each factor on drawdown characteristics.

5.1 Parameter h_c

To explore the influence of parameter h_c, defined as the vertical distance from the bottom of the retaining wall to the top of the impermeable layer, on the groundwater drawdown distribution around the excavation wall, the groundwater drawdown distributions at $t = 100$ d were calculated for three cases with h_c set to 10, 20, and 30 m, respectively, as shown in Fig. 5. It is observed that the groundwater levels exhibit significant variations near the bottom of the wall on both sides. With an increasing value of parameter h_c, the groundwater drawdown distribution lines both inside and outside the retaining wall shift upward, showing a notable drawdown difference particularly in the far-field region of the seepage field, while the variation near the inner boundary adjacent to the retaining wall remains relatively minor. Furthermore, Fig. 6 depicts the temporal drawdown changes at a representative monitoring location ($x = 27, z = h_o$) outside the excavation pit, clearly indicating that the penetration depth of the waterproof curtain does not considerably affect the time required to reach a stable drawdown. However, an increase in penetration depth of the waterproof curtain (corresponding to a decrease in parameter h_c) significantly reduces groundwater drawdown at the monitoring point. Specifically, as the value of h_c decreases from 30 to 10 m, the groundwater drawdown at this location is reduced by approximately 52%.

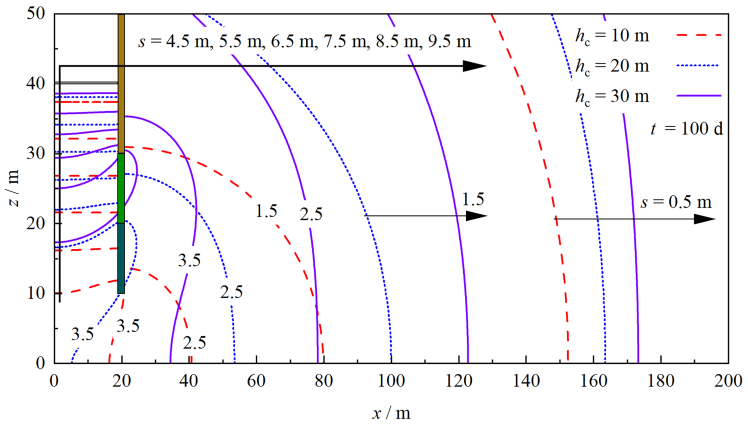

Figure 5: Influence of parameter h_c on the drawdown distribution inside and outside foundation pit

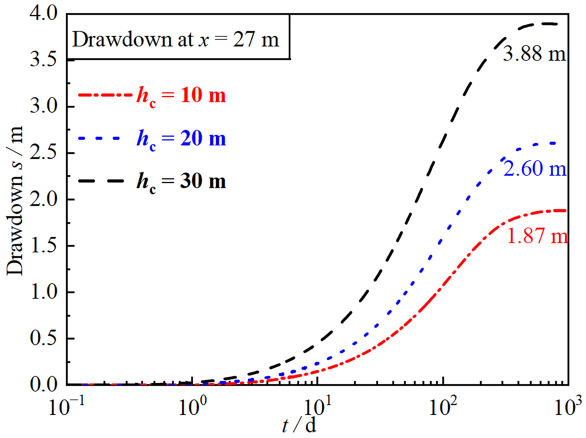

Figure 6: Influence of parameter h_c on the drawdown at monitoring point outside the pit

5.2 Thickness of the Waterproof Curtain

To investigate the influence of the waterproof curtain thickness (denoted as parameter d) on groundwater drawdown distribution around the excavation retaining wall, the groundwater drawdown profiles at $t = 100$ d were computed for three cases: d $\rightarrow$ 0 m (representing the scenario without considering the wall thickness), $d = 3$ m, and $d = 6$ m, respectively, as illustrated in Fig. 7. It is worth noting that in practical engineering, the thickness of reinforced concrete diaphragm walls or suspended waterproof curtains is typically designed within the range of 0.5–2.0 m, while thicker sections may be adopted in special cases such as deep or large-scale excavations. Therefore, the values selected in this study (up to 6 m) cover and extend beyond the common engineering practice, providing a broader perspective for sensitivity analysis [7]. The results demonstrate that as the thickness of the waterproof curtain increases, the groundwater drawdown inside the retaining wall gradually decreases, while the equipotential lines in the far-field outside the excavation progressively shift leftward. Additionally, near the outer side of the retaining wall, equipotential lines exhibit intersection phenomena with increasing wall thickness. Moreover, Fig. 8 illustrates the temporal evolution of groundwater drawdown at a monitoring point outside the excavation pit under varying curtain thicknesses. It is observed that the waterproof curtain thickness does not substantially affect the time required for seepage to reach a steady state. Nevertheless, its influence on groundwater drawdown is predominantly noticeable during the later stages of seepage, where an increase in curtain thickness progressively reduces drawdown magnitude. This indicates that an increase in waterproof curtain thickness effectively modifies groundwater seepage pathways, thus helping mitigate the risk of seepage-induced failures in excavation projects.

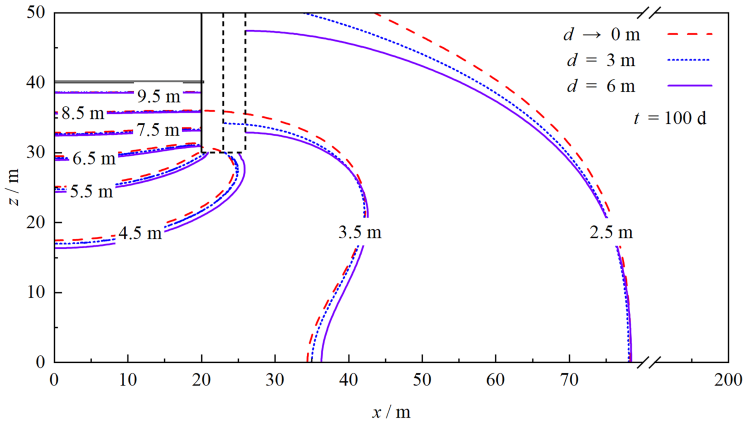

Figure 7: Influence of parameter d on the drawdown distribution inside and outside foundation pit

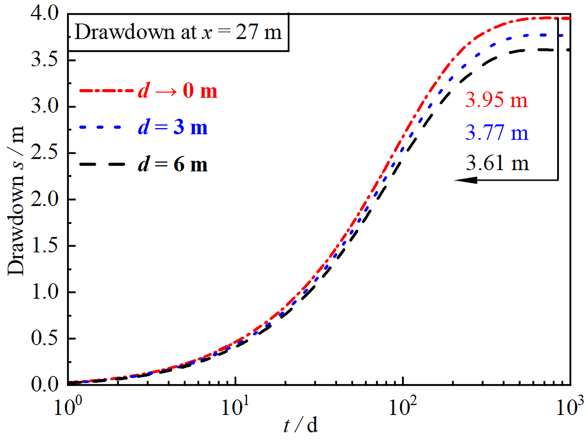

Figure 8: Influence of parameter d on the drawdown at monitoring point outside the pit

5.3 Specific Yield S_Y

Fig. 9 compares the groundwater drawdown at the monitoring location ($x = 27, z = h_o$) for three different specific yield (S_Y) scenarios. In practical hydrogeological conditions, the specific yield of soils generally falls in the range of 0.1–0.4, with lower values corresponding to fine-grained soils (e.g., silts and clays) and higher values typical of sandy or gravelly aquifers. Evidently, the drawdown-time relationships exhibit a pronounced nonlinear pattern, reflecting the delayed influence of the specific yield on groundwater release. Initially, the drawdown develops rapidly, closely matching the theoretical prediction considering only elastic storage (represented by the scenario $S_Y \rightarrow 0$). With increasing pumping duration, the groundwater drawdown rate noticeably slows due to the delayed mobilization and gradual release of water stored by the specific yield. Ultimately, the groundwater drawdown stabilizes at lower magnitudes for higher specific yield values. For instance, increasing S_Y from 0.2 to 0.4 leads to a considerable reduction in drawdown magnitude, underscoring the critical role of delayed yield release in offsetting water table declines during extended dewatering operations.

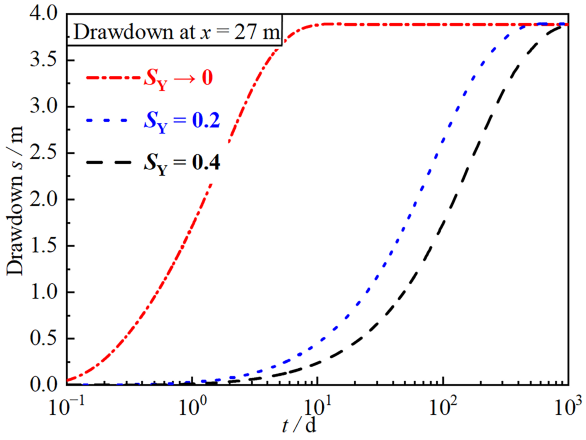

Figure 9: Influence of parameter S_Y on the drawdown at monitoring point outside the pit

5.4 Parameter h_i

To further elucidate the influence of the excavation-side water level (denoted as parameter h_i) on the total head distribution around the retaining wall, Fig. 10 presents the computed equipotential contours at $t = 100$ d for three representative cases: $h_i = 30$, 35, and 40 m. The results indicate that the hydraulic gradient is particularly steep near the base of the retaining wall, as evidenced by the dense clustering of drawdown contours in this region, which reflects the pronounced change in seepage potential across the wall interface. As the internal water level h_i increases, the equipotential lines for drawdown on the external side of the wall shift markedly towards the excavation, indicating a more pronounced decrease in water level outside the pit. Simultaneously, the internal equipotential lines also move upward, reflecting a greater magnitude of drawdown within the excavation. Overall, an increase in h_i leads to a substantial rise in drawdown both inside and outside the wall, with an expanded region of influence for the drawdown. A higher internal water level results in a greater hydraulic head difference, which intensifies seepage around the excavation and significantly amplifies both the extent and the magnitude of the drawdown response.

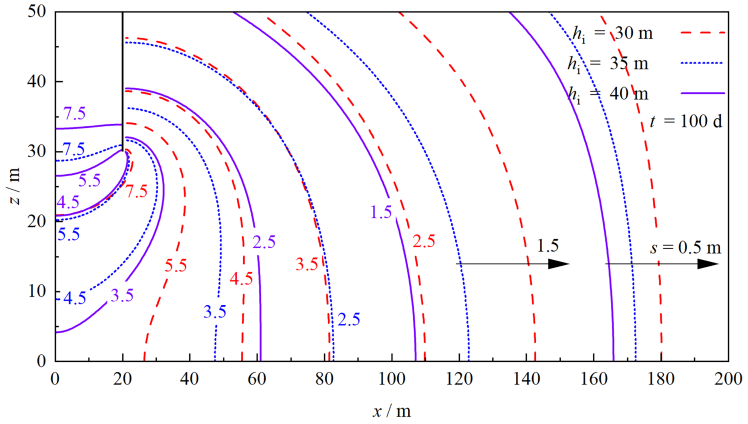

Figure 10: Influence of parameter h_i on the drawdown distribution inside and outside foundation pit

In addition, beyond providing theoretical insights, the semi-analytical model developed in this study has the potential to be extended into design-oriented tools. The parametric results presented

herein can serve as a basis for developing practical design charts in future studies, thereby strengthening the link between theoretical modeling and engineering application.

6 Conclusions

In this study, a theoretical framework was established to investigate transient groundwater seepage in foundation pits featuring a phreatic surface, with explicit consideration of the influences of waterproof curtain penetration depth, curtain thickness, and specific yield. The proposed semi-analytical solution was rigorously validated through comparison with both laboratory experimental results and high-fidelity numerical simulations, ensuring its accuracy and reliability. Furthermore, a series of parametric analyses was conducted to systematically explore the effects of these key parameters on the spatial and temporal characteristics of groundwater drawdown. The principal findings of this research are summarized as follows:

(1) Both the vertical distance from the retaining wall base to the top of the impermeable layer (h_c) and the thickness (d) of the waterproof curtain are key factors controlling the spatial characteristics of groundwater drawdown. Reducing h_c from 30 to 10 m lowers the external groundwater drawdown by approximately 52%. Conversely, increasing the curtain thickness from 0 to 6 m decreases the steady-state drawdown at the monitoring point outside the pit by more than 8%. These results indicate that curtain geometry plays a decisive role in mitigating adverse dewatering impacts.

(2) The specific yield (S_Y) exerts a significant influence on the temporal evolution of groundwater drawdown. Greater values of S_Y cause the drawdown curve to flatten over time, resulting in a slower rate of decline and a reduced final drawdown magnitude. This underscores the role of delayed gravity drainage in modulating aquifer responses under transient seepage conditions.

(3) Elevating the internal water level (h_i) inside the excavation increases the hydraulic head differential across the pit, which not only broadens the range of the seepage-affected zone but also intensifies drawdown responses both inside and outside the retaining wall. This finding highlights the importance of managing internal water levels to control seepage patterns and associated risks in deep excavation projects.

Overall, these results reveal the underlying mechanisms: the penetration depth governs the extent of the hydraulic connection between the excavation and aquifer; the curtain thickness primarily alters the seepage pathways and resistance; the specific yield controls the rate of delayed water release; and the internal water level drives the hydraulic gradient that determines the intensity and spread of drawdown. Together, these mechanisms explain how design and operational parameters interact to shape the spatial–temporal evolution of the seepage field, providing both theoretical insights and practical guidance for foundation pit engineering.

Nevertheless, some limitations of the present study should be noted. The waterproof curtain was idealized as a perfect hydraulic barrier, whereas in real engineering applications, construction defects or material heterogeneity may allow partial seepage. In addition, the analytical framework is primarily applicable to rectangular excavations with a length-to-width ratio greater than 5. For more irregular or complex pit geometries, numerical simulation methods provide a more flexible tool and can be employed to complement the analytical framework. Future research could therefore focus on relaxing the impermeable curtain assumption by introducing partially permeable boundary conditions and on extending the present model in combination with numerical simulations to handle more general excavation layouts, thereby improving its robustness and practical applicability.

Acknowledgement: This work was supported by the Hezhou University. We gratefully acknowledge the Guangxi Heyuan Technology Development Co., Ltd. and Guangxi Construction Engineering Group No. 3 Construction Engineering Co., Ltd. for providing the necessary techniques for this study.

Funding Statement: This work had been supported by the Fund Project: the Guangxi Science and Technology Plan Project (GuiKe AD23026035); the Doctoral Research Start-up Fund of Hezhou University (HZUBS202207); the Guangxi Natural Science Foundation of China (No. 2024GXNSFBA010173); the Hezhou Science and Technology Development Project (Heke2024120); the Hezhou Foundation for Research and Development of science and Technology (No. 2024124); the Hezhou Foundation for Research and Development of science and Technology (No. 2024125). Guangxi University Engineering Research Center for Green and Low-Carbon Urban Regeneration Construction.

Author Contributions: The authors confirm contribution to the paper as follows: study conception and design: Donglin Meng, Jingjing Han; data collection: Wenkai Lei, Haifeng Zhang, Changzan Guan; analysis and interpretation of results: Donglin Meng, Haifeng Zhang; draft manuscript preparation: Donglin Meng, Jingjing Han. All authors reviewed the results and approved the final version of the manuscript.

Availability of Data and Materials: Due to the nature of this research, participants of this study did not agree for their data to be shared publicly, so supporting data is not available.

Ethics Approval: Not applicable.

Conflicts of Interest: The authors declare no conflicts of interest to report regarding the present study.

References

1. Li D, Zhao Y, Liu N, Jiao L, Liu Z. Evaluation and analysis of seepage stability in the surrounding strata of a dewatering foundation pit based on differences in particle initiation conditions. Indian Geotech J. 2025;55:622–35. doi:10.1007/s40098-024-01000-w.
2. Yang Q, Chen S. Research on the deformation mechanism and law caused by the influence of seepage on foundation pit dewatering. Front Earth Sci. 2025;12:1523165. doi:10.3389/feart.2024.1523165.
3. Yang W, Xu J. One-dimensional consolidation of multilayered aquifer systems with viscoelastic properties induced by time-dependent groundwater drawdown. Q J Eng Geol Hydrogeol. 2022;55(2):qjegh2021-73. doi:10.1144/qjegh2021-073.
4. Yang W, Xiao L, Tang Z, Mei G. An improved theoretical method for assessing tunnel response to pre-excavation dewatering: time-dependent deflection, internal force, joint opening, and dislocation. Comput Geotech. 2025;183:107216. doi:10.1016/j.compgeo.2025.107216.
5. Yang W, Xiao L, Mei G. A general solution of consolidation for a double-layer foundation soil induced by pre-excavation dewatering with bottom reinforcement considering delayed responses of water table. Phys Fluids. 2024;36:117160. doi:10.1063/5.0234101.
6. Yang W, Ni P, Chen Z, Feng J, Mei G. Consolidation analysis of composite ground improved by granular piles with a high replacement ratio considering overlapping smear zones. Comput Geotech. 2023;162:105636. doi:10.1016/j.compgeo.2023.105636.
7. Huang R, Ni P, Yang W, Chen Z, Dong Q, Mei G. Semianalytical solution for consolidation of reclaimed land with horizontal drains. Int J Geomech. 2023;23:4023010. doi:10.1061/IJGNAI.GMENG-7921.

8. Huang J, He Z, Yu J, He W. Analytical solutions and application of circular cofferdams considering backseal effects. Chin J Geotech Eng. 2023;45:2510–8. doi:10.11779/CJGE20221101.
9. Yu J, Li D, Hu Z, Zheng J. Analytical solution of steady seepage field of foundation pit considering thickness of retaining wall. Chin J Geotech Eng. 2023;45:1402–11. (In Chinese). doi:10.11779/CJGE20220357.
10. Yu J, Yang X, Deng P, Chen W. Analytical solution for a steady seepage field of a foundation pit in layered soil. Int J Geomech. 2022;22(10):4022160. doi:10.1061/(ASCE)GM.1943-5622.0002496.
11. Li K, Chen S, Pei R, Chen J. Theoretical prediction study on drawdown and surface settlement induced by dewatering and excavation in unconfined aquifers. Comput Geotech. 2025;179:107041. doi:10.1016/j.compgeo.2024.107041.
12. Ying H, Nie W, Huang D. Semi-analytical solution of pore pressure response around excavations to groundwater level fluctuation. Chin J Geotech Eng. 2014;36:1012–9. (In Chinese). doi:10.11779/CJGE201406004.
13. Ying H, Nie W, Huang D. Influences of groundwater level fluctuation on the stability of gravity retaining wall of pits. Chin J Rock Mech Eng. 2014;33:2370–6. doi:10.13722/j.cnki.jrme.2014.11.021.
14. Yu J, Zhang Z, Zheng J, He Z. Analytical solution of pore pressure in seepage field of foundation pit with bottom seal under water level fluctuation. Rock Soil Mech. 2023;44:3415–23. (In Chinese). doi:10.16285/j.rsm.2023.0322.
15. Sun G, Yang Y, Cheng S, Zheng H. Phreatic line calculation and stability analysis of slopes under the combined effect of reservoir water level fluctuations and rainfall. Can Geotech J. 2017;54(5):631–45. doi:10.1139/cgj-2016-0315.
16. Zheng Y, Shi W, Kong W. Calculation of seepage forces and phreatic surface under drawdown conditions. Chin J Rock Mech Eng. 2004;23(18):3203–10. (In Chinese). doi:10.3321/j.issn:1000-6915.2004.18.031.
17. Yu J, Zhang Y, Zheng J, Zhang Z. Analytical solution of two-dimensional steady-state seepage field in a pit considering a diving surface. Rock Soil Mech. 2023;44:3109–16. (In Chinese). doi:10.16285/j.rsm.2022.2019.
18. Neuman SP. Theory of flow in unconfined aquifers considering delayed response of the water table. Water Resour Res. 1972;8(4):1031–45. doi:10.1029/WR008i004p01031.
19. Neuman SP. Effect of partial penetration on flow in unconfined aquifers considering delayed gravity response. Water Resour Res. 1974;10(2):303–12. doi:10.1029/WR010i002p00303.
20. Xu J, Liu L, Zhang H. Drawdown-induced consolidation of aquifer systems considering water-table decline. Int J Numer Anal Methods Geomech. 2023;47(11):2049–63. doi:10.1002/nag.3550.
21. Yang W, Xiao L, Mei G. A semi-analytical solution for seepage field and soil deformation induced by coupled pre-excavation dewatering and groundwater recharge with a suspended waterproof curtain considering delayed phreatic surface response. Adv Water Resour. 2025;206:105111. doi:10.1016/j.advwatres.2025.105111.
22. Chen Z, Ni P, Chen Y, Mei G. Plane-strain consolidation theory with distributed drainage boundary. Acta Geotech. 2020;15(2):489–508. doi:10.1007/s11440-018-0712-z.
23. Chen Z, Ni P, Zhu X, Mei G. Using boundary transform method to solve geotechnical problems with mixed-type boundary conditions. J Geotech Geoenviron Eng. 2022;148(12):6022013. doi:10.1061/(ASCE)GT.1943-5606.0002921.
24. Yang W, Qiu C, Duan Y, Feng J, Mei G. One-dimensional consolidation analysis of layered foundations subjected to arbitrary loads under a continuous drainage boundary. Int J Geomech. 2024;24(6):04024091. doi:10.1061/IJGNAI.GMENG-9317.
25. Chen Z, Ni P, Mei G, Chen Y. Semi-analytical solution for consolidation of ground with partially penetrating PVDs under the free-strain condition. J Eng Mech. 2021;147(2):4020148. doi:10.1061/(ASCE)EM.1943-7889.0001884.
26. Xiao T, Ni P, Chen Z, Feng J, Chen D, Mei G. A semi-analytical solution for consolidation of ground with local permeable pipe pile. Comput Geotech. 2022;143(11):104590. doi:10.1016/j.compgeo.2021.104590.

27. Li T, Sun D, Chen Z, Wang L. Semi-analytical solution for two-dimensional contaminant transport through composite liner with strip defects. Constr Build Mater. 2024;440(8):137404. doi:10.1016/j.conbuildmat.2024.137404.
28. Duan Y, Wu W, Wang T, Yang W, Qiu C, Mei G. A semi-analytical solution for consolidation of soft ground improved by locally permeable pipe piles under time-dependent loads. Comput Geotech. 2023;163(1):105750. doi:10.1016/j.compgeo.2023.105750.
29. Abate J, Whitt W. A unified framework for numerically inverting laplace transforms. INFORMS J Comput. 2006;18(4):408–21. doi:10.1287/ijoc.1050.0137.
30. Stehfest H. Algorithm 368: numerical inversion of laplace transforms [D5]. Commun ACM. 1970;13(1):47–9. doi:10.1145/361953.361969.
31. Zhao X, Guo N, Cao W, Gong W, Liu Y. Semi-analytical solution for double-layered elliptical cylindrical foundation model improved by prefabricated vertical drains. Int J Numer Anal Methods Geomech. 2024;48(7):1833–45. doi:10.1002/nag.3711.
32. Wang J, Deng Y, Ma R, Liu X, Guo Q, Liu S, et al. Model test on partial expansion in stratified subsidence during foundation pit dewatering. J Hydrol. 2018;557:489–508. doi:10.1016/j.jhydrol.2017.12.046.
33. He G, Yan X, Zhang Y, Yang T, Wu J, Bai Y, et al. Experimental study on the vertical deformation of soils due to groundwater withdrawal. Int J Geomech. 2020;20(7):04020076. doi:10.1061/(ASCE)GM.1943-5622.0001709.
34. Xue L, Yang B, Liu F, Zhang B, Wang K. Model test system for groundwater seepage in foundation pit engineering. Chin J Geotech Eng. 2017;39(s1):126–131. (In Chinese). doi:10.11779/CJGE2017S1025.